Plasma Properties and Performance of Mercury Ion Thrusters

T. D. MASEK*

Jet Propulsion Laboratory, Pasadena, Calif.

The objectives of this paper are 1) to present a description of the electron bombardment ion thruster operation, 2) to show the relationship of the plasma to this operation, and 3) to present a consistent method for computing the discharge power per beam ion from the plasma properties for comparison with the measured value. A modified form of the Bohm stable sheath criterion is shown to apply for computing fluxes. The use of this criterion, along with calculations of ion production rates and electron fluxes, permits a more accurate and comprehensive picture of discharge losses than has been obtained previously. Langmuir probe measurements in conventional 15- and 20-cm-diam thrusters using mercury are presented. The 15-cm-diam thruster, of 1962 vintage, was operated at high flowrates (650 ma equivalent mercury flowrate) for comparison with previous lower flow-rate data and to establish reference thruster plasma characteristics.

I. Introduction

QUANTITATIVE or analytical relationships between the plasma properties and operation of mercury thrusters have been of interest for some time.[1,2] Previous studies have indicated the difficulty of obtaining useful analytical expressions describing over-all thruster operation.[2,3] To obtain analytical solutions requires, in general, a great number of assumptions because of the complex nature of the plasma. The non-Maxwellian electron velocity distribution function in mercury, nonuniform applied magnetic fields, an unknown neutral atom density distribution, and general mathematical difficulties all severely restrict the validity, and, hence, the usefulness of analytical solutions. On the other hand, experimental studies of plasma properties,[4,5] although providing quantitative data at specific operating points, have not heretofore provided the desired relationships between these properties and thruster operating parameters.

This paper presents a description of thruster operation, based on plasma measurements, that is consistent with gross thruster measurements[6,7] (i.e., beam current and discharge losses). A method is described for computing ion beam current and discharge losses from measurements of ion density and electron temperature. As a part of these calculations, the ion flux to the discharge chamber walls, the electron current to the anode, and the ion production rate are found.

The data required for this study were obtained with movable Langmuir probes in 15- and 20-cm-diam thrusters. Data published previously,[8] as well as new measurements, are presented for the unimproved 15-cm-diam thruster. All improved thruster data were obtained with a 20-cm-diam thruster. Experimental setups have been reported previously[8,9] for both thrusters and are not described herein.

II. Fundamentals of Operation

A. General Operation

A description of the general features of this type of thruster is required to discuss the mechanisms controlling bombardment thruster operation in detail. Figure 1 illustrates the processes involved in producing and accelerating ions.

Electrons are accelerated away from the cathode by an electric field (produced by the discharge voltage) and collide with atoms, ions, and other electrons. The resulting low-pressure discharge (approximately 10^{-3} torr) would ordinarily allow long mean-free paths for electrons. However, an axial magnetic field is provided to restrict the radial motion of the electrons. This field gives electrons a long cycloidal path with a cyclotron radius of the order of 1 cm. Electrons are inhibited from reaching the walls, which are held at cathode potential, by the wall sheath. Because they spiral around the field lines, electrons require collisions to obtain a radial drift velocity. The ionization process depends upon the electron energy, electron density, and atom density. The mean energy of an electron depends on both the electron density and the discharge voltage and is a major factor in efficient thruster operation. The factors controlling electron energy, or more specifically the electron velocity distribution function, are basic to the plasma.

As in all low-pressure plasmas of this type with relatively large anodes, the plasma potential is generally positive with respect to the anode.[10] Since this potential also appears at the cathode sheath, electrons initially enter the plasma with

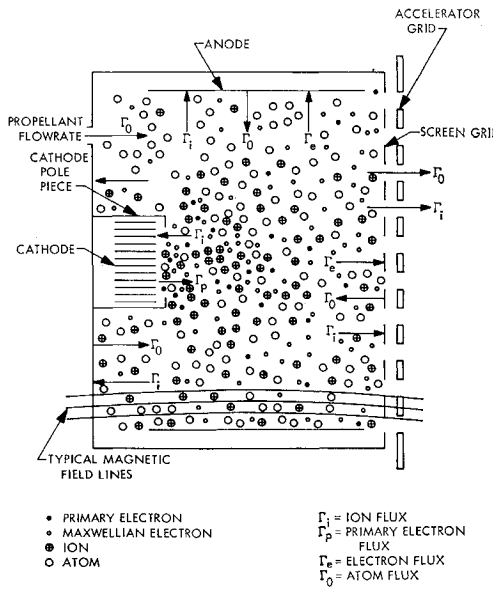

Fig. 1 Thruster and plasma schematic diagram.

Presented as Paper 69-256 at the AIAA 7th Electric Propulsion Conference, Williamsburgh, Va., March 3–5, 1969; submitted March 21, 1969; revision received July 20, 1970. This paper presents the results of one phase of research carried out in the Research and Advanced Concepts Section of the Jet Propulsion Laboratory, California Institute of Technology, under Contract NAS7-100, sponsored by NASA. The author acknowledges the valuable assistance of the Applications Studies Group Laboratory Staff in making the experimental measurements, and the helpful suggestions and critical review of the paper by D. J. Kerrisk.

* Member of the Technical Staff. Member AIAA.

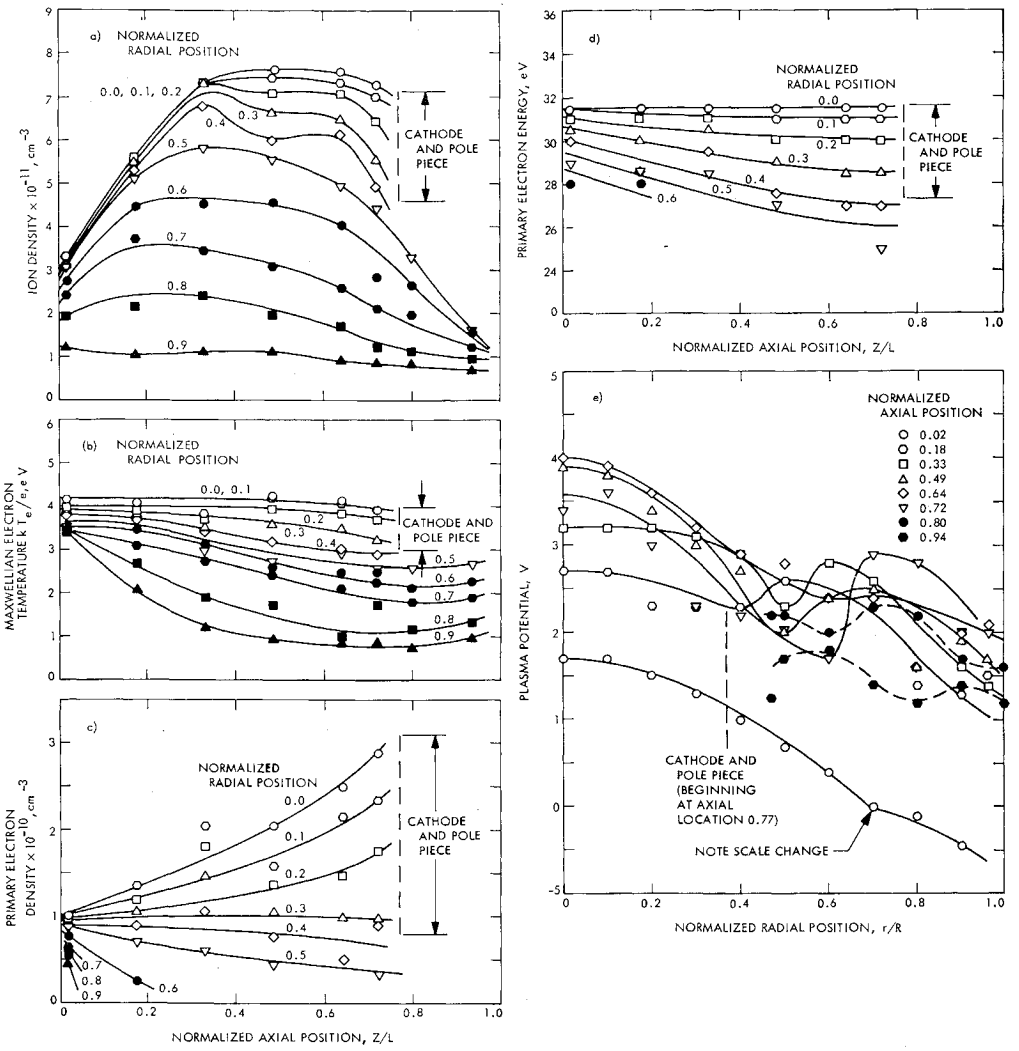

Fig. 2 Plasma properties in the 20-cm-diam thruster: flowrate, 9.0 g/hr; propellant utilization efficiency, 88%.

energies slightly higher than the discharge voltage (35–45 v for conventional mercury thrusters).

These initial electrons, primary electrons, are shown as black dots in Fig. 1. Collisions between electrons, or inelastic collisions of primary electrons with atoms or ions, redistribute the primary electron energy. Electrons produced in ionization, or thermalized primary electrons, can be considered to form a second distinct group (small open circles in Fig. 1). This group in general has a Maxwellian distribution function, although variations from Maxwellian have been observed.[5] A combination of these two groups is commonly found in the bombardment thruster. Although the primary electron density is low (less than 10% of the total electron density), the primary electrons usually contribute approximately half of the ionization.

Ionization occurs for the most part in a one-step process from the atomic ground state. Ionization from excited states is relatively infrequent because transition times[11] (approximately 10^{-7} sec) are much shorter than electron-atom collision times[2] (approximately 5×10^{-5} sec for 30-ev primary electrons and a neutral density of 10^{12} cm^{-3}).

Ion motion is determined primarily by the plasma potential. This can be verified by considering ion collisions with electrons, ions, and atoms. (Note that the magnetic field has little influence as indicated by ion cyclotron radii of the order of meters.) For collisions with electrons when the electron speed is much higher than the ion speed, the momentum exchange per collision, divided by the ion momentum, is given approximately by[12]

$$\Delta(m_i v_i)/m_i v_i = (m_e \epsilon_e / m_i \epsilon_i)^{1/2} \quad (1)$$

where m is the particle mass, ϵ the energy, v the speed, and the subscripts i and e refer to ions and electrons, respectively. Thus, for typical mercury conditions $\epsilon_e/\epsilon_i = 100$, $m_e/m_i = 2.7 \times 10^{-6}$, the ion momentum changes only approximately 1.6% per electron collision. Although up to approximately 50 collisions occur per centimeter of ion path length,[2] the net force applied to the ion by these electron impacts should be small because of the randomness of the electron velocities. Therefore, the ion motion is essentially unaffected by collisions with electrons.

The largest cross section for ion-atom collisions is that for charge exchange. For an ion speed of 3×10^4 cm/sec, typical of thermal ions, this cross section is approximately 2×10^{-14} cm^2 (Ref. 13). With a typical atom density of 10^{12} cm^{-3}, the mean-free path is 50 cm and is much greater than ordinary thruster dimensions.

Ion-ion collisions are not important. Ions are accelerated in the general direction of the maximum plasma potential gradient. Because all ions at a given position are moving in the same general direction, collisions should have a small effect on ion motion. A portion of the ions flow toward the accelerating grids, cross the plasma sheath at the screen grid, and accelerate through several kilovolts. The remaining ion flux goes to the anode, housing, screen grid, and cathode.

Ions reaching the walls recombine to form atoms, which evaporate along with the atoms reaching the surfaces directly, to form a virtual propellant source. The evaporating atoms have velocities corresponding to typical wall temperatures of 150–250°C. The magnitude of this source was shown to be of the same magnitude as the main propellant flowrate.[14]

The cost of producing ions ϵ_i, determined by dividing the discharge power by the beam current, can be expressed as the product of two factors:

$$\epsilon_i = \omega\epsilon_b, \text{ ev/beam ion} \quad (2)$$

where ϵ_b is the basic cost of producing ions in the plasma and ω is the ratio of total ion flux (wall flux plus beam flux) to beam ion flux. Both ϵ_b and ω depend on the plasma characteristics and thruster configuration. Calculations of ω and ϵ_b are presented in the following sections.

B. Ion Fluxes

Since plasma ion motion is determined almost entirely by the plasma potential distribution, the ion fluxes cannot be computed by usual diffusion theory methods. However, a direct method is available through use of the Bohm stable sheath criterion.[15] This criterion establishes the minimum ion energy, normal to the sheath, necessary to form a stable sheath. In normal thruster operation, the sheaths are stable and the Bohm criterion can be expected to apply. In the case of a Maxwellian electron distribution, this minimum energy was shown to be $kT_e/2e$ (i.e., half the electron temperature at the sheath). The presence of primary electrons modifies this ion energy slightly. As shown in Ref. 14, the minimum possible ion energy at the sheath, when primary electrons are present, is

$$\epsilon_i = kT_e/2e\ (n_i/n_m) \quad (3)$$

where n_m is the Maxwellian electron density, n_i the ion density, and T_e the temperature of the Maxwellian electrons. In the present calculations, the density ratio in Eq. (3) differs significantly from unity only at the screen grid and cathode.

To verify the validity of the criterion given in Eq. (3), the ion flux through the screen grid computed from plasma properties can be compared with the measured ion beam current.

1. *Beam flux*

By using Eq. (3), the beam current can be written as

$$I_b = 2\pi e\phi_i \int_0^R n_i(r,0)v_i(r,0)rdr \quad (4)$$

where

$$v_i(r,z) = \{kT_e(r,z)/m_i[n_i(r,z)/n_m(r,z)]\}^{1/2} \quad (5)$$

The term ϕ_i accounts for screen grid blockage, and $n_i(r,0)$ is the ion density at the screen grid. The integration can be replaced with a summation to obtain

$$I_b = e\phi_i \sum_j (n_i v_i)_j A_j \quad (6)$$

where A_j is a concentric segment of grid area. This approximation by a summation is consistent with the possible experimental errors in n_i and v_i.

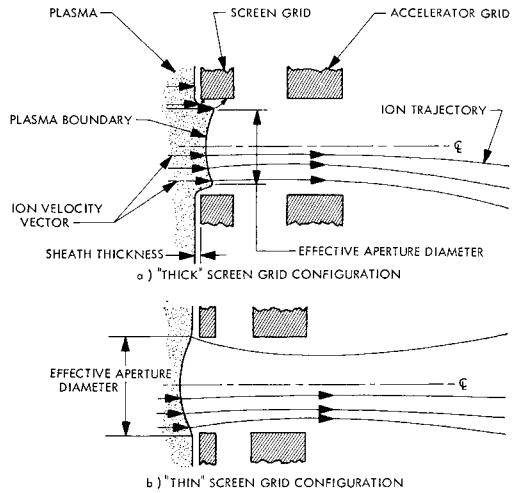

Fig. 3 Plasma sheath screen grid boundary configurations.

Typical distributions of Maxwellian and primary electron density, plasma potential, primary electron energy, and Maxwellian electron temperature obtained with Langmuir probes are shown in Fig. 2 for the 20-cm-diam thruster. Additional data are presented in Ref. 14 for the 15-cm- and 20-cm-diam thrusters. In the 15-cm-diam thruster, the electron energy distribution was entirely Maxwellian within experimental error. This is attributed to the high plasma density operation needed to obtain beam current densities equivalent to the present 20-cm-diam thruster (approximately 3 ma/cm^2). The ratio of primary electron density to ion density in the 20-cm-diam thruster is relatively uniform at the screen grid. Therefore, an average value of n_i/n_m was used in the calculations. It should be noted that, in the 20-cm-diam thruster, the cathode was mounted on a pole piece (Fig. 1). This element was not used in the 15-cm-diam thruster.

The comparison of the measured and calculated beam currents was made by computing the value of ϕ_i needed to give the correct beam current. The value of ϕ_i should be approximately equal to the fraction of screen-grid open area corrected for sheath effects. The results of calculations using the data in Fig. 2, as well as six additional sets for the 20-cm-diam thruster and four sets for the 15-cm-diam thruster, are shown in Table 1. Since measurements were not taken at the sheath, the data were extrapolated to this position. The values of ϕ_i calculated for the 20-cm-diam thruster are quite close to the fraction of screen-grid open area of approximately 0.72 (1385 apertures of 0.462-cm-diameter in a 20-cm-diam area). In the 15-cm-diam thruster cases, the calculated ϕ_i value is approximately 0.38 compared with the grid open-area fraction of approximately 0.48 (475 apertures of 0.475-cm-diameter in a 15-cm-diam area). This difference is directly attributable to the plasma boundary configurations as shown in Fig. 3.

Table 1 Comparison of ion flux from Bohm criteria with beam current

Parameter	15-cm-diam thruster				20-cm-diam thruster						
	1	2	3	4	1	2	3	4	5	6	7
Beam current, a	0.50	0.55	0.21	0.23	0.68	0.83	1.06	1.09	0.72	0.85	0.96
Bohm ion flux, a	1.35	1.44	0.54	0.62	0.90	1.10	1.41	1.48	0.95	1.15	1.30
ϕ_i	0.37	0.38	0.39	0.37	0.75	0.75	0.75	0.74	0.76	0.74	0.74
Corrected screen-grid open-area fraction	0.40	0.40	0.40	0.40	0.72	0.72	0.72	0.72	0.72	0.72	0.72
Propellant flow-rate, g/hr	4.7	4.7	1.9	1.9	5.7	6.9	9.0	9.2	9.2	9.2	9.2
Utilization efficiency, %	77.0	88.0	85.0	91.0	89.0	90.0	88.0	89.0	58.0	68.0	78.0

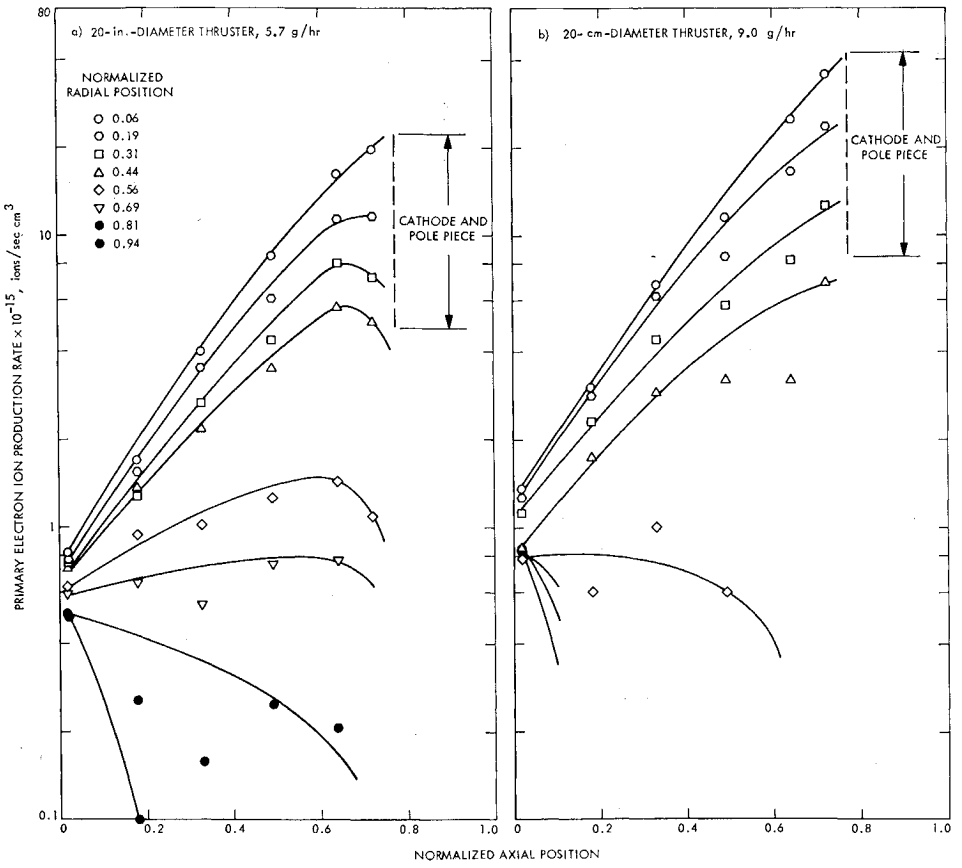

Fig. 4 Local ion production rate by Maxwellian and primary electrons.

The major accelerator-system differences between the 15-cm- and 20-cm-diam thrusters studied were the screen grid thickness and the screen-accelerator grid spacing, as indicated in Table 1. The plasma boundary configuration of the 15-cm-diam thruster should correspond to Fig. 3a, which shows a relatively thick screen with wide spacing. In general, the plasma boundary position adjusts to supply the demanded space-charge-limited current. The space-charge-limited current is inversely proportional to the square of the accelerator-plasma boundary spacing. For a given ion flux density from the plasma, the accelerator-plasma boundary spacing will decrease with decreasing space-charge-limited current. For the 15-cm-diam thruster, this boundary position appears to be within the aperture. Boundary shapes similar to those in Fig. 3 have been found in computer studies of ion optics.[16]

With the plasma boundary located within the aperture (Fig. 3a), the effective diameter of the aperture is reduced by approximately twice the plasma-screen grid sheath thickness. Most ions crossing the boundary between the edge of the aperture and the boundary inflection point will be accelerated into the screen grid. The sheath thickness (see Fig. 3) can be estimated by equating the space-charge-limited ion current arriving at the screen to the ion flux from the plasma. For a planar geometry, we have

$$4\epsilon_0/9(2e/m_i)^{1/2}(V_s^{3/2}/x^2) = en_iv_i \qquad (7)$$

where V is the plasma potential with respect to the screen, x the sheath thickness, and $\epsilon_0 = 8.85 \times 10^{-12}$ coul/nm^2. Solving for x, obtaining v_i from Eq. (5),

$$x = \left[\frac{4}{9}\frac{\epsilon_0}{e}\left(\frac{2e}{kT_e}\right)^{1/2}\left(\frac{n_m}{n_i}\right)^{1/2}\frac{V_s^{3/2}}{n_i}\right]^{1/2}, m \qquad (8)$$

Using average plasma conditions at the sheath ($V_s = 35$v, $kT_e/e = 4$ ev, $n_i = 10^{11}$ cm^{-3}, and $n_m/n_i = 0.95$) and consistent units, Eq. (8) gives a sheath thickness of approximately 2×10^{-2} cm. The effective aperture diameter in this case (for the 15-cm-diam thruster) is approximately 0.435 cm, resulting in an effective open-area fraction of 0.40, which is in good agreement with the values calculated from the Bohm ion flux.

A thin screen grid and close grid spacing should produce a plasma boundary similar to that shown in Fig. 3b. It should be noted that in this case, ϕ_i could be greater than the grid open-area fraction. This interpretation of the plasma boundary-shape change with screen grid thickness is also consistent with efficiency improvements previously observed in tests on the 20-cm-diam thruster.[7]

From the agreement of the calculated value of ϕ_i with the corrected grid open-area fraction, it can be concluded that, within the experimental accuracy of the present data, the ion velocity at the sheath is given by the modified Bohm criterion. Ion fluxes to the anode, cathode, and housing can now be computed using this ion velocity and the plasma conditions at the location of interest.

2. *Wall flux*

The factor ω in Eq. (2) is the ratio of the total ion flux (to all boundaries including the beam) to the beam current. The ion current to any surface in the thruster can be calculated by integrating the flux (en_iv_i) over that surface. As before, this integration was accomplished by summing the flux contributions to segments of area. The anode, housing, rear chamber surface, cathode, and cathode pole piece surfaces were divided into segments. The size of the segment was chosen to be consistent with the variation of (n_iv_i) along that segment. The values of n_i and v_i (or kT_e/e) at the surface (i.e., the sheath at the surface) were found, as before, by extrapolating the experimental data graphically to the surface and using the Bohm criterion.

The results of these calculations, using the data of Fig. 2 as well as three additional data sets for the 20-cm-diam thruster

and three sets for the 15-cm-diam thruster, are shown in Table 2. The values of ω thus computed allow ϵ_b to be found since ϵ_t is known. These values of ϵ_b are also given in Table 2. A comparison of the 15-cm- and 20-cm-diam thruster results, and a discussion of the relationship of these to performance, will be presented later in this paper.

C. Electron Flux

The total flux of electrons to the walls must balance the total ion flux for all surfaces but the anode. The net current to the housing (cathode, pole piece, rear surface, screen grid, etc.) must be zero. Total electron current to the anode is the sum of the discharge, beam, and ion currents. Since the discharge and beam currents are directly measured, a calculation of the electron current to the anode should verify the previous ion flux calculation.

The anode sheath retards electron flow and is similar to that of a negatively biased Langmuir probe. Thus, to first order, the electron flux to the anode is given by

$$\Gamma_e = [(n_e\bar{v}_e)_s/4]e^{-\alpha_1^2} \tag{9}$$

where $\alpha_1 = v_s/c_e$

$$c_e = (2kT_e/m_e)^{1/2} = (\pi/2)^{1/2}\bar{v}_e$$

and v_s is the minimum electron velocity, in a direction normal to the sheath, needed to overcome the sheath potential. The ratio of electron to ion fluxes, from Eqs. (5) and (9), is

$$\Gamma_e/\Gamma_i = 244e^{-\alpha_1^2} \tag{10}$$

Since density and temperature drop out of Eq. (10), and Γ_i is already known, finding the value of this ratio is equivalent to finding Γ_e.

The flux ratio is not necessarily constant along the anode. Thus, the flux ratio at a given location probably does not equal the total current ratio (I_e/I_i). Equation (10) was evaluated for each anode area segment as in the ion flux calculations. These values were averaged by area and summed to obtain the average total current ratio. The calculated values of (I_e/I_i) and the measured values, found by taking the ratio of total electron current (discharge, beam, and ion currents) to calculated ion current, agreed within 10% (Ref. 14), which was well within the experimental accuracy. This shows that the calculations of electron and ion flux are consistent.

D. Ion Production Rate

The total ion production rate within the plasma must equal the total ion flux. Thus, a direct calculation of the ion production rate is a second method for evaluating ω and ϵ_b.

With the assumption that ionization occurs only from the ground state, the ion production rate can be found from previous calculations by Kerrisk.[17] The ion production rate can be written in the form[2]

$$\dot{\nu}_i = n_0[n_m\Sigma_m + n_p\Sigma_p], \text{ ions/sec cm}^3 \tag{11}$$

Table 2 Summary of ion wall-flux calculations

Parameter	15-cm-diam thruster 1	2	3	20-cm-diam thruster 1	2	3	4
Ion flux, a	...	...	...	...	...	...	...
Beam	0.50	0.55	0.21	0.68	0.83	1.06	1.09
Screen grid	0.85	0.90	0.33	0.23	0.27	0.35	0.38
Anode	0.72	0.85	0.20	0.27	0.37	0.45	0.46
Housing	1.30	1.42	0.18	0.30	0.35	0.46	0.48
Cathode	0.42	0.42	0.30	0.24	0.40	0.51	0.57
Cathode pole piece	...	...	...	0.23	0.33	0.37	0.38
Total ion flux, a	3.79	4.14	1.22	1.95	2.55	3.20	3.36
ϵ_t, ev/beam ion	828.0	890.0	640.0	178.0	186.0	194.0	192.0
ω	7.58	7.55	5.80	2.87	3.08	3.02	3.08
ϵ_b, ev/plasma ion	109.0	118.0	110.0	62.0	61.0	64.0	62.0

Table 3 Summary of ion production-rate calculations

Parameter	15-cm-diam thruster 1	2	20-cm-diam thruster 1	2	3	4
Beam current, a	0.50	0.55	0.68	0.83	1.06	1.09
ϕ_0	0.5	0.5	0.44	0.44	0.44	0.44
$n_0(r_0, 0) \times 10^{-11}$, cm^{-3}	12.0	7.6	4.8	5.2	8.0	7.0
Total ion production rate, a	4.5	4.5	1.8	2.8	2.9	3.6
ω	9.0	8.2	2.7	3.4	2.7	3.3
ϵ_t	828.0	890.0	178.0	186.0	194.0	192.0
ϵ_b	92.0	109.0	66.0	55.0	69.0	58.0

where Σ_m and Σ_p are coefficients for Maxwellian and primary electrons, respectively, and n_0 is the neutral atom density. It should be noted that the densities and coefficients in Eq. (11) are functions of position, and that $\dot{\nu}_i$ must be integrated (or summed) over the plasma volume to find the total ion production rate.

A major difficulty in evaluating $\dot{\nu}_i$ is that n_0 is unknown. A first-order estimate of this density was made in Ref. 14, based on the loss of neutrals through the accelerator system. Applying Eq. (11) and the referenced calculation of n_0 to the data sets used in the previous section, the local ion production rates were computed. The local rates were multiplied by volume elements and summed to find the total rate. The values of ω and ϵ_b, so determined, are presented in Table 3. The reasonably good agreement between the results in Tables 2 and 3 gives increased confidence in both methods. However, the crude atom density calculation places an upper limit on the confidence in the ion production method.

Having confirmed the general accuracy of the total ion production rate, the distribution of local rates should be noted. These rates, from both Maxwellian and primary electrons, are shown in Fig. 4 for data from the 20-cm-diam thruster. The ionization rate due to primary electrons is shown in Fig. 5. The figure illustrates that primary electrons contribute substantially to the total ion production.

E. Ion Production Cost

The basic mechanisms for energy loss from the plasma can be discussed by considering the energy lost by electrons. This is possible because the discharge power is initially totally contained in the electron energy. Electrons lose energy mainly in inelastic collisions with atoms and ions and in collisions with chamber surfaces. Elastic collision losses are quite small. The sum of the inelastic collisional loss and the surface loss will be compared with the total discharge loss.

The chamber (anode and other housing potential surfaces) losses can be estimated as follows. The average electron energy transported across the sheath can be found by integrating over the electron velocity distribution function for electron energies greater than the sheath potential V_s. Near the walls, the electron velocity distribution function is generally Maxwellian (see Fig. 2). The average electron energy flux reaching the wall is given by

$$q_e = (2kT_e/e)e\Gamma_eG, W \tag{12}$$

where

$$G = 1 - [(\pi)^{1/2}/2]\alpha_1[1 - \text{erf}(\alpha_1)]e^{\alpha_1^2}$$

and other terms were defined for Eq. (9). The factor G does not vary greatly from unity and, in the present analysis, will be taken equal to unity. It should be noted that $e\Gamma_e$ is just the electron current to the wall.

The chamber losses can be computed from Eq. (12) using the previously tabulated wall fluxes. These losses are given in Table 4 for the anode and housing surfaces. The housing loss neglects the effect of primary electrons. Average Max-

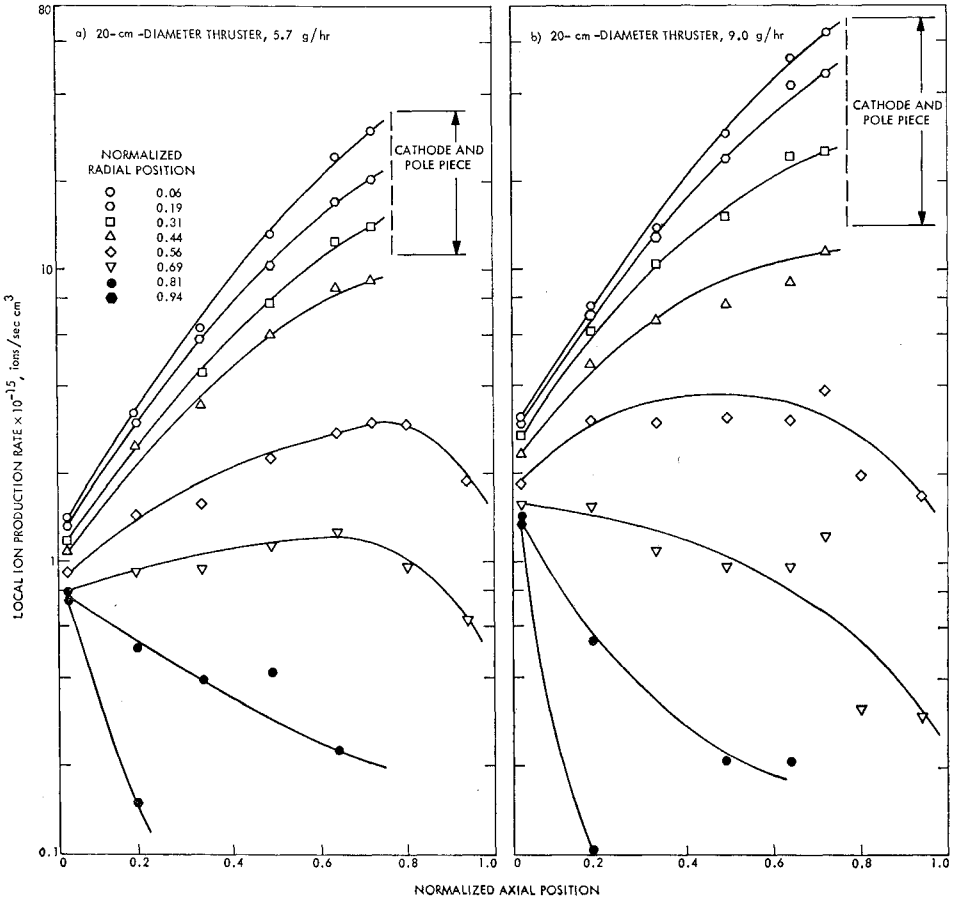

Fig. 5 Local ion production rate by primary electrons.

wellian electron temperatures near the walls were used for the calculations.

The average energy loss due to inelastic electron collisions ϵ_c(ev/plasma ion) can be estimated by considering the energy lost in ionization and excitation of atoms and ions. For the present density range, most of the energy going into excitation should be radiated to the walls.[18] The local collisional loss, ϵ_c', which will be a function of position in the plasma, is written in the form

$$\epsilon_c' = V_i + \left[\sum_j \langle Q_j(\epsilon_e)\epsilon_e^{1/2}\rangle V_j + (n_i/n_0)\sum_k \langle Q_k(\epsilon_e)\epsilon_e^{1/2}\rangle V_k / \langle Q_i(\epsilon_e)\epsilon_e^{1/2}\rangle\right] \quad (13)$$

where V_i is the ionization potential, V_j the energy of the jth atomic state, V_k the energy of the kth ion state, Q_i the ionization cross section, Q_j the atom excitation cross section for state j, Q_k the ion excitation cross section for the state k, ϵ_e is the electron energy, and the brackets indicate an integration over the energy distribution function. Thus, in the right-hand term of Eq. (13), the numerator represents the excitation loss and the denominator represents the ionization rate.

The excitation loss in Eq. (13) was evaluated for Maxwellian and primary electron energy distributions. The atom excitation terms were evaluated for the 6^1P_1 and 6^3P_1 states, which have transitions to the ground state. The cross sections for these distributions were taken from Ref. 19. Other atomic terms should be small. Ion excitation cross sections were not available; however, the ion contribution can be estimated. Line intensities for ion transitions[20] are small except for the 1942 Å and 2345 Å lines. The intensity of these lines is about the same as for the $^1P_1$ (1849 Å) atom line.

As an estimate of the ion excitation contribution to ϵ_c', the ion excitation loss was taken to be equal to that for the $^1P_1$ atom state. A value of n_i/n_0 equal to unity was used in computing the curves of Fig. 6. The curves could be expected to shift upward or downward as n_i/n_0 is increased or decreased. The ion production rates were computed from the Σ_m and Σ_p coefficients. The results are consistent with similar calculations of Dugan and Sovie[18] for cesium, argon, and helium. The mercury (V_i = 10.39 ev) curves lie between those for cesium (V_i = 3.87 ev) and argon (V_i = 15.76 ev).

The average loss ϵ_c cannot be evaluated directly because the Maxwellian electron temperature and primary electron energy distribution vary spacially (i.e., ϵ_c' varies spacially). The contributions to ionization at a given position must be weighted by volume. The discharge power should equal the integrated product over the chamber of $\epsilon_c'\dot{\nu}_i$ plus the anode and housing loss. Using the data presented previously in preparing Table 3, $\epsilon_c'\dot{\nu}_i$ was summed over the chamber volume elements to obtain the results shown in Table 4. This calculation of the discharge power resulted in values within 20% of the measured power. This is a reasonable agreement considering that the ϵ_c' curves used (Fig. 6) do not account for changes in n_i/n_0.

III. Discussion

The previous analysis provided relationships for relating the plasma properties to thruster performance. The fundamental importance of the discharge loss factors ω and ϵ_b was demonstrated. The validity of the Bohm criterion for calculating wall ion fluxes and the wall loss factor ω were verified by computing 1) the ion beam current, 2) the total ion production rate, and 3) the anode current. The basic cost of ion production ϵ_b was shown to be the sum of electron inelastic collisional (radiation and ionization) losses and electron energy transport to the walls.

Improvements in thruster performance must involve the factors ω and ϵ_b. This is illustrated in Table 2. Considering the Bohm criterion, ω is reduced by 1) increasing the ratio of effective screen-grid open area to wall area, 2) selectively increasing the electron temperature in the grid region or decreasing this temperature at the walls, and 3) selectively increasing the ion density in the grid region or reducing this density at the walls. The basic ion production cost depends on electron energy flux losses and collisional losses. The electron energy flux loss is reduced by reducing the wall flux and reducing the electron temperature at the wall. The collisional loss is reduced by decreasing the ion density (since $\epsilon_c'\nu_i$ is proportional to ion density), and increasing the electron energy throughout the plasma. It is noted that selective reductions in ion density can decrease both ω and ϵ_b. However, a reduction in electron energy to reduce the wall flux will result in a large increase in ϵ_c'. This indicates that the lower limit on discharge losses will be determined primarily by the trade-off of wall losses and basic ion production costs.

IV. Conclusions

The analysis presented in this paper was successful in establishing the basic relationships between the plasma properties and thruster discharge performance. The following conclusions can be drawn from this work.

1) The ion velocity, determined by the modified Bohm criterion and applied at the screen-grid sheath, produces the measured beam current. This result was used to compute total ion flux to the beam and walls. An independent calculation of the total ion flux, using the total ion production rate, verified the Bohm calculation.

2) The principal plasma losses, contributing to the ion production cost per plasma ion ϵ_b, were shown to be inelastic collisional losses (resulting in excitation and subsequent radiation) and electron energy transport to the anode. In present thrusters, the collisional losses (atoms and ions) contribute approximately 90% of the total loss. A lower limit on the value of ϵ_b can be made from this result. The lower limit on the collisional loss (Fig. 6) appears to be approximately 20 ev/plasma ion. Therefore, considering the housing and anode losses, a limiting value for ϵ_b of approximately 30 ev/plasma ion can be expected. However, this low basic cost may not be consistent with a low ion wall loss factor since a high electron energy is required for low ϵ_b. Therefore, a value of 40 ev/plasma ion is a more realistic estimate for the achievable limit on ϵ_b.

3) Additional reductions in the ion wall loss factor seem possible. Increases in screen-grid open-area fraction should be the most direct approach. Obvious mechanical difficulties restrict this possible improvement. Direct insulation of the housing surfaces, or ion trapping (by use of magnetic fields as demonstrated by Moore in Ref. 21), may reduce the wall loss fraction. Values of ω less than approximately 1.5 seem unlikely. In this case, a lower limit on total discharge losses of approximately 60 ev/beam ion seems probable. However, for conventional thrusters without ion trapping, a limit on ω of approximately 2 is expected. This indicates a lower limit on discharge losses of approximately 80 ev/beam ion for the conventional thruster.

Table 4 Electron energy losses

Parameter	15-cm-diam thruster		20-cm-diam thruster			
	1	2	1	2	3	4
Anode loss, w	53	62	8	10	11	17
Housing loss, w	17	20	5	6	6	6
Collisional loss, w	290	350	120	166	210	214
Discharge power, w	413	490	122	154	206	209
ϵ_a, ev/plasma ion	14	15	4	4	3	5
ϵ_h, ev/plasma ion	5	5	2	2	2	2
ϵ_c, ev/plasma ion	76	85	60	65	66	66
Theoretical ϵ_b	95	105	66	71	71	73

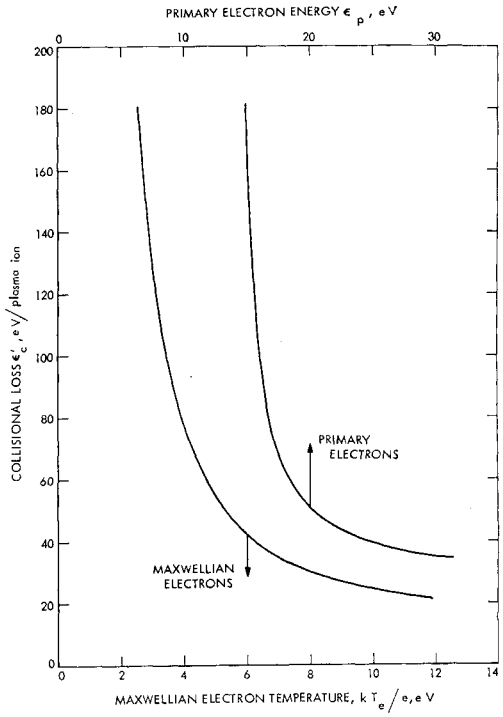

Fig. 6 Local collisional energy loss factor.

4) The higher discharge losses observed using a hollow cathode, compared to an oxide cathode, are directly related to ion losses to the interior surfaces of the pole piece. Reduction of this surface area, by insulation or size reduction, is expected to improve hollow cathode thruster performance.

5) Comparison of the basic losses for mercury and cesium thrusters, using data from Ref. 1 for cesium thrusters and Ref. 17 for ϵ_c', shows little difference between these propellants. It is noted that, although ionization potentials are quite different for cesium and mercury, the electron temperature in the plasma is proportional to the ionization potential. Therefore, a direct comparison of propellants for the present thruster must consider plasma properties as well as the physical properties of the propellant.

References

[1] Kohlberg, I. and Nablo, S., "Physical Phenomena in Bombardment Ion Sources," *Physics and Technology of Ion Motors*, edited by F. E. Marble and J. Surugue, Gordon and Breach Science Publishers, New York, 1966.

[2] Masek, T. D., "Plasma Characteristics of Electron Bombardment Ion Engines," TR 32-1271, April 1968, Jet Propulsion Lab., Pasadena, Calif.; also presented at the 2nd International Conference on Electron and Ion Beam Science and Technology, New York, April 1966.

[3] Kaufman, H. R., "Performance Correlation for Electron-Bombardment Ion Sources," TN D-3041, Oct. 1965, NASA.

[4] Strickfaden, W. B. and Geiler, K. L., "Probe Measurements of the Discharge in an Operating Electron Bombardment Engine," TR 32-417, Jet Propulsion Lab., Pasadena, Calif.; also *AIAA Journal*, Vol. 1, No. 8, Aug. 1963, pp. 1815–1823.

[5] Masek, T. D., "Plasma Studies in the Electron Bombardment Ion Engine," Space Programs Summary 37-42, Vol. IV, Nov. 31, 1965; Space Programs Summary 37-44, Vol. IV, March 31, 1966, Jet Propulsion Lab., Pasadena, Calif.

[6] Masek, T. D. and Womack, J. R., "Experimental Studies with a Mercury Bombardment Ion Engine System," AIAA Paper 67-698, Colorado Springs, Colo., 1967; also TR 32-1280, July 1968, Jet Propulsion Lab., Pasadena, Calif.

[7] Masek, T. D. and Pawlik, E. V., "Thrust System Technology for Solar Electric Propulsion," *AIAA Journal*, Vol. 6, No. 5, May 1969, pp. 557–564.

[8] Kerrisk, D. J. and Masek, T. D., "Effects of Plasma Non-Uniformity on Grid Erosion in an Electron Bombardment Ion Engine," *AIAA Journal*, Vol. 3, No. 6, June 1965, pp. 1060–1066; also TR 32-727, July 1965, Jet Propulsion Lab., Pasadena, Calif.

[9] Masek, T. D., "Plasma Investigation in the SE-20C Thruster," Space Programs Summary 37–53, Vol. III, Jet Propulsion Lab., Pasadena, Calif., Oct. 31, 1968.

[10] Langmuir, I., "The Interaction of Electron and Positive Ion Space Charges in Cathode Sheaths," *Physical Review*, Vol. 33, 954, 1929 pp. 954–989.

[11] Mitchell, A. C. G. and Zemansky, M. W., *Resonance Radiation and Excited Atoms*, Cambridge University Press, 1961.

[12] Sutton, G. W. and Sherman, A., *Engineering Magnetohydrodynamics*, McGraw-Hill, New York, 1965.

[13] Rapp, D. and Francis, W. E., "Charge Exchange Between Gaseous Ions and Atoms," *Journal of Chemical Physics*, Vol. 37, 1962, pp. 2631–2645.

[14] Masek, T. D., "Plasma Properties and Performance of Mercury Ion Thrusters," AIAA Paper 69-256, Williamsburg, Va., 1969.

[15] Bohm, D., "Minimum Ionic Kinetic Energy for a Stable Sheath," *The Characteristics of Electrical Discharges in Magnetic Fields*, edited by A. Guthrie and R. K. Wakerling, McGraw-Hill, New York, 1959, pp. 77–86.

[16] Brewer, G. R. et al., "Ion Engine Thrust Vector Study," Quarterly Rept. No. 1, Phase II, Jet Propulsion Lab. Contract 952129, Dec. 1968, Hughes Research Labs., Malibu, Calif.

[17] Kerrisk, D. J., "Arc-Type Ion Sources for Electrical Propulsion," TN 61-4, May 1961, Aeronautical Systems Div., Wright-Patterson Air Force Base, Dayton, Ohio.

[18] Dugan, J. V. and Sovie, R. J., "Volume Ion Production Costs in Tenuous Plasmas," TN 4-4150, Sept. 1967, NASA.

[19] Arnot, F. L. and Baines, G. O., "Elastic and Inelastic Cross Sections of the Mercury Atom," *Proceedings of the Royal Society*, A151, 1935, pp. 256–274.

[20] *Handbook of Chemistry and Physics*, The Chemical Rubber Publishing Co., Cleveland, Ohio, 1962.

[21] Moore, D. R., "Magneto-Electrostatic Bounded Plasma Ion Thruster," AIAA Paper 69-260, Williamsburg, Va., 1969.

FEBRUARY 1971 AIAA JOURNAL VOL. 9, NO. 2

Sequential Estimation of the State and the Observation-Error Covariance Matrix

BYRON D. TAPLEY*
The University of Texas at Austin, Austin, Texas

AND

GEORGE H. BORN†
NASA Manned Spacecraft Center, Houston, Texas

The simultaneous maximum-likelihood estimate of the observation-error covariance matrix and the state is developed in sequential form. The resulting estimator requires only an approximate initial estimate for the observation-error covariance matrix, and the estimator uses the observation data to refine and update the initial estimate. Simulated observation data of a near-Earth satellite are used to evaluate the estimation scheme. The observation vector consists of a simultaneous measurement of range, azimuth, and elevation for a spacecraft during one pass over a tracking station. The results of the numerical simulation indicate that if the a priori value for the observation-error covariance matrix is in error, the performance of the estimation algorithm is significantly improved when the covariance matrix is estimated.

Nomenclature

$A(t)$ = $n \times n$ matrix of time-dependent coefficients
C = constant
cof = cofactor
F = log of the likelihood function
$f(x,y;R)$ = joint density function
H = mapping matrix
I = identity matrix
i,j,k,l,N,p = indices
$L(x,R)$ = likelihood function
P = estimation-error covariance matrix
R = observation-error covariance matrix
$\hat{R}_0$ = initial guess of R
R_T = true value of R
t = time
v = observation-noise vector
W = weighting function
X = true state
X^* = reference state
x = state deviation
Y = actual observation
y = observation deviation
$y_1,\ldots,y_N$ = set of observation deviations
σ = standard deviation
σ^2 = variance
ϕ = null matrix
$\Phi(t_k,t_j)$ = state transition matrix
$(\hat{\ })$ = best estimate
$(\ )^*$ = evaluated on the reference trajectory

Subscript

0 = initial value

Superscript

T = transpose

Operators

E = expected value
$(\dot{\ })$ = differentiation with respect to time

Received September 25, 1969; revision received May 20, 1970. This investigation was partially supported by NASA under Contract NAS-9-6963 and NGR 44-012-008.

* Professor and Chairman, Department of Aerospace Engineering and Engineering Mechanics. Member AIAA.

† Special Assistant to Chief, Theory and Analysis Office, Computation and Analysis Division; now at Jet Propulsion Laboratory, Pasadena, California. Member AIAA.